Biomaterials 301 (2023) 122272

Contents lists available at ScienceDirect

Biomaterials

journal homepage: www.elsevier.com/locate/biomaterials

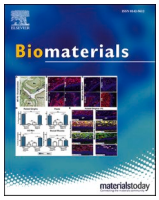

Structurally decoupled stiffness and solute transport in multi-arm poly (ethylene glycol) hydrogels

Nathan R. Richbourg [a,*], Nicholas A. Peppas [a,b,c,d,**]

[a] Department of Biomedical Engineering, University of Texas, Austin, TX, 78712, USA
[b] McKetta Department of Chemical Engineering, University of Texas, Austin, TX, 78712, USA
[c] Division of Molecular Therapeutics and Drug Delivery, College of Pharmacy, University of Texas, Austin, TX, 78712, USA
[d] Departments of Surgery and Pediatrics, Dell Medical School, University of Texas, Austin, TX, 78712, USA

ARTICLE INFO

Keywords:
Hydrogel network structure
Solute transport
Junction functionality
Swollen polymer network model
poly(ethylene glycol) (PEG)

ABSTRACT

Synthetic hydrogels are widely used as artificial 3D environments for cell culture, facilitating the controlled study of cell-environment interactions. However, most hydrogels are limited in their ability to represent the physical properties of biological tissues because stiffness and solute transport properties in hydrogels are closely correlated. Resultingly, experimental investigations of cell-environment interactions in hydrogels are confounded by simultaneous changes in multiple physical properties. Here, we overcame this limitation by simultaneously manipulating four structural parameters to synthesize a library of multi-arm poly (ethylene glycol) (PEG) hydrogel formulations with robustly decoupled stiffness and solute transport. This structural design approach avoids chemical alterations or additions to the network that might have unanticipated effects on encapsulated cells. An algorithm created to statistically evaluate stiffness-transport decoupling within the dataset identified 46 of the 73 synthesized formulations as robustly decoupled. We show that the swollen polymer network model accurately predicts 11 out of 12 structure-property relationships, suggesting that this approach to decoupling stiffness and solute transport in hydrogels is fundamentally validated and potentially broadly applicable. Furthermore, the unprecedented control of hydrogel network structure provided by multi-arm PEG hydrogels confirmed several fundamental modeling assumptions. This study enables nuanced hydrogel design for uncompromised investigation of cell-environment interactions.

1. Introduction

Cell-encapsulating 3D hydrogels have led to new insights about cell-environment interactions that drive stem cell differentiation and modulate healthy cell and cancer cell behaviors [1–6]. The influence of hydrogel stiffness on stem cell differentiation is well-documented, with mesenchymal stem cells biasing their differentiation toward cell types appropriate for tissues with stiffnesses that match their environment [7–10]. This stiffness-differentiation correlation has motivated many studies of how hydrogels with different stiffnesses affect encapsulated cells, including studies of secondary mechanical influences such as viscoelasticity [11–17]. However, recent studies are increasingly considering how solute transport within a 3D hydrogel structure affects cell behavior [18–28]. The knowledge that stiffness and solute diffusivity both affect encapsulated cell behaviors indicates a need for robust methods of decoupling stiffness and solute diffusivity in hydrogels to precisely investigate how cells interact with their environment [18–20].

Poly (ethylene glycol) diacrylate (PEGDA) hydrogels, a commonly used "blank slate," non-biochemically active material for 3D cell encapsulation, have a strong correlation between tensile moduli and mesh size (a parameter used to represent how hydrogel structure affects solute transport) [24,25,29–34]. We note that mesh size is an inconsistently reported and incomplete representation of solute transport within hydrogels and instead directly measure and report solute diffusion coefficients within hydrogels in this study [35–37]. Browning et al. [29] and Munoz-Pinto et al. [30] both aimed to decouple stiffness and solute transport in PEGDA hydrogels, but both approaches were functionally limited. Browning et al. incorporated four-arm PEG acrylates into PEGDA, mixing tetrafunctional junctions with radically polymerized acrylate chains. Their approach changed the network structure and

* Corresponding author. Department of Biomedical Engineering, University of Texas, Austin, TX, 78712, USA.
** Corresponding author. Department of Biomedical Engineering, University of Texas, Austin, TX, 78712, USA.
E-mail addresses: nrichbourg@utexas.edu (N.R. Richbourg), peppas@che.utexas.edu (N.A. Peppas).

https://doi.org/10.1016/j.biomaterials.2023.122272
Received 15 March 2023; Received in revised form 1 August 2023; Accepted 7 August 2023
Available online 9 August 2023

physical properties while maintaining a consistent PEG backbone, but their final comparison of tensile modulus and mesh size still showed a universal curve relating modulus and mesh size. While they identified extreme conditions where either the tensile modulus changed but not the mesh size or the mesh size changed but not the tensile modulus, they were not able to decouple stiffness and solute transport for the intermediate values or create hydrogels with both high stiffness and high solute transport.

Munoz-Pinto et al. [30] incorporated *N*-vinyl pyrrolidone (NVP) into PEGDA networks. Adding NVP shifted the modulus-mesh size curves toward higher values for both properties, decoupling stiffness and solute transport compared to PEGDA hydrogels without NVP. However, introducing NVP changed the chemical nature of the hydrogel and may not translate effectively to hydrogels based on other polymers. The Browning et al. and Munoz-Pinto et al. studies highlight the need for a way to decouple stiffness and solute transport in hydrogels without relying on a mechanism unique to a single type of hydrogel or a second polymer that introduces different chemical properties to the hydrogel. A broadly applicable structural approach to decoupling stiffness and solute transport in hydrogels is needed.

Here, we used a network structure-based approach to decouple stiffness and solute diffusivity in multi-arm poly (ethylene glycol) (PEG) hydrogels. Critically, multi-arm PEG hydrogels provide more robust control of network structure than PEGDA-only hydrogels, which form radically polymerized kinetic chain junctions with undefined functionalities [38–44]. After synthesizing hydrogel formulations with simultaneous variations in four structural parameters, we measured their stiffnesses and solute transport profiles with small and large solutes [35–37,45–47]. We confirmed decoupled stiffness and solute transport using an unbiased statistical algorithm. Comparisons with swollen polymer network model predictions showed consistent trends for each structural parameter-property pairing except for the degree of polymerization between junctions and solute transport, a PEG-specific deviation that enhanced the observed decoupling of stiffness and solute transport. Our results validate a structural approach to decoupling stiffness and diffusivity in multi-arm PEG hydrogels that enables the design of nuanced cell-encapsulating hydrogels for studying cell-environment interactions.

2. Results & discussion

2.1. Structural hydrogel design approach

To investigate whether hydrogel structure can be manipulated to decouple stiffness and solute transport properties, we created a library of multi-arm PEG hydrogel formulations, each formulation having a unique combination of four structural parameters (Fig. 1A). Three values for each structural parameter were selected to produce a wide range of physical properties, constrained by the availability of multi-arm PEG precursors and the expected limits of gelation. A set of nine multi-arm PEG precursor macromers was selected with 4, 6, or 8 arms (corresponding to junction functionality f) and average arm lengths of 2.5, 3.75, and 5 kDa to yield degrees of polymerization between junctions (N_j) of approximately 115, 165, and 215 repeating units upon cross-linking. Because two PEG arms are linked together by a small cross-linking molecule (DTT), the degree of polymerization between junctions

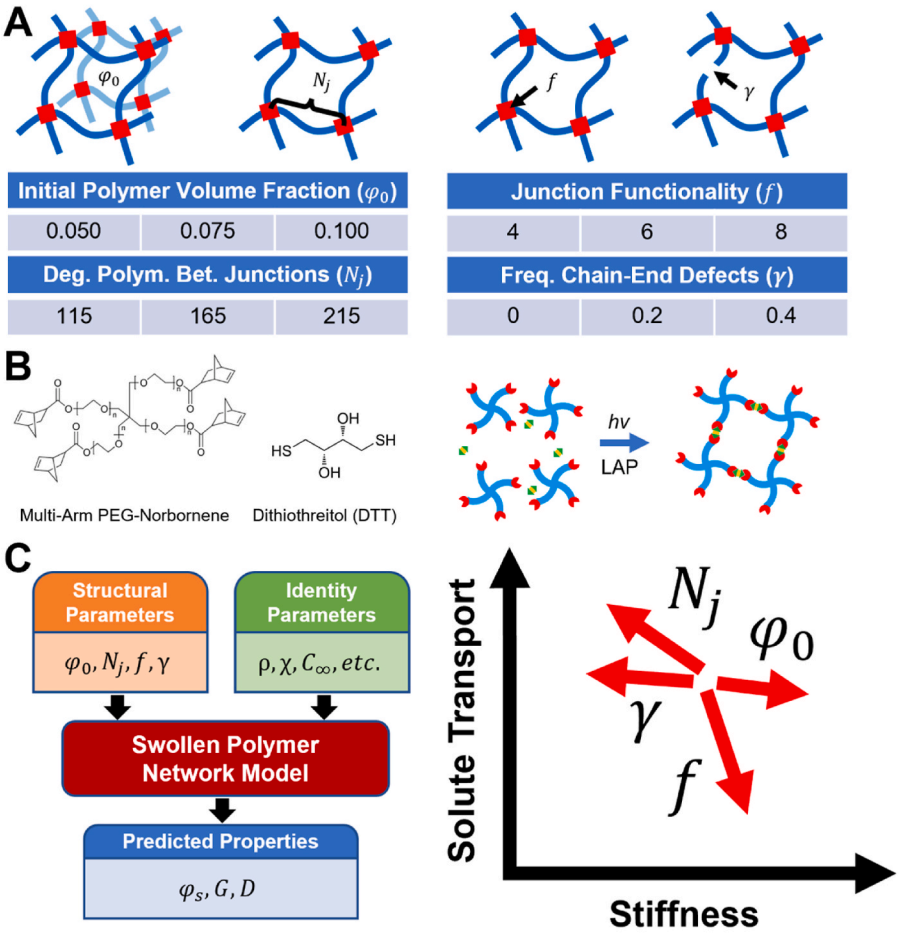

Fig. 1. Model-driven approach for structurally decoupling stiffness and solute transport in multi-arm PEG hydrogels. (A) Four structural parameters, each with three values, were simultaneously varied to form a library of 81 multi-arm PEG hydrogel formulations. (B) The LAP and UV light-initiated reaction between PEG-norbornene macromers and DTT to form multi-arm PEG hydrogels. (C) Summary of the swollen polymer network modeling approach used to predict how structural parameters affect hydrogel stiffness and solute transport. Specific predictions of structure-property interactions across the 81 formulations are shown in Supp. Fig. S1.

is approximately twice the degree of polymerization per PEG arm. All PEG macromers were end-functionalized with norbornene groups and then synthesized into hydrogel formulations using dithiothreitol (DTT) as a crosslinking agent and Lithium phenyl-2,4,6-trimethylbenzoylphosphinate (LAP) as a photoinitiator of the efficient thiol-norbornene click reaction (Fig. 1B) [35,39,40]. Hydrogels were synthesized at three initial polymer volume fractions ($\varphi_0 = 0.050, 0.075, 0.100$). Finally, the stoichiometric ratio of DTT thiol groups to norbornene groups was varied (1:1, 0.8:1, 0.6:1) to control the frequency of chain-end defects ($\gamma = 0, 0.2, 0.4$). These four quantitative structural parameters were selected because 1) they are explicitly included in the swollen polymer network model, enabling *a priori* prediction of physical properties (Fig. 1C, Supp. Fig. S1), 2) they are independently controlled via synthesis conditions, facilitating clear structure-function analysis, and 3) they are not specific to a single polymer or crosslinking scheme, indicating that their influences on hydrogel properties are potentially applicable to many kinds of hydrogels [36,46].

In total, 81 hydrogel formulations were initially planned based on the full matrix of four parameters with three values each. Critically, stiffness and solute transport predictions for each hydrogel formulation, made using the swollen polymer network model (equations provided in the Experimental Section), suggested that the structural variations would decouple stiffness and solute transport across the set of formulations (Fig. 1C, Supp. Fig. S1). Two formulations were not synthesized due to limited low yield from the norbornene functionalization of the 6-arm, 3.75 kDa per arm PEG macromer (Formulations A6-N165-V050-F04 and A6-N165-V075-F04). Six other formulations failed to form intact hydrogels, despite boundaries based on previous studies in multi-arm PEG hydrogels [41] (A4-N115-V050-F04, A4-N165-V050-F04, A4-N215-V050-F04, A4-N215-V075-F04, A4-N215-V100-F04, A8-N165-V050-F04). Therefore, only 73 of the planned 81 hydrogel formulations were synthesized and fully characterized. All six of the non-gelling formulations had the highest frequency of chain-end defects ($\gamma = 0.4$). While a high frequency of chain-end defects was the most consistent feature of formulations that failed gelation, 19 formulations with $\gamma = 0.4$ formed intact hydrogels, suggesting that all four structural parameters contributed to formulation-dependent gelation failures. Generally, a higher frequency of chain-end defects, a lower junction functionality, a lower initial polymer volume fraction, and a higher degree of polymerization between junctions increased the likelihood of a formulation failing gelation. Further analysis via Flory-Stockmayer percolation theory may better explain these limitations [48].

2.2. Hydrogel stiffness-swelling relationship

Following the rubberlike elasticity theory, hydrogel equilibrium swelling and stiffness are expected to be highly correlated [46]. The swollen polymer model predictions, which are based on equilibrium swelling theory and rubberlike elasticity theory, precisely reflect this correlation (Fig. 2). The measured correlation between independently measured hydrogel stiffness and swelling (swollen polymer volume fraction) matches the overall trend across the 73 hydrogel formulations (Fig. 2). However, swollen polymer volume fractions and stiffnesses trended much higher in the measurements than predicted, and the correlation between swelling and stiffness was looser than predicted.

The perfect predicted correlation between stiffness and swelling is based on the modeling assumption that only the concentration of elastically active chains within a network (and the junction functionality-dependent phantom network distortion) determines the stiffness of the network [46]. In other words, the length of the chains in the network does not directly affect the stiffness, assuming they are in a Gaussian distribution and long enough to act as entropic springs. Whether this assumption is true cannot be explicitly confirmed or denied based on the data, partially because it requires a more rigorous accounting for the real number of elastically active chains than presented here [49]. The chain lengths would likely need to be varied more broadly than the three values here to distinguish a chain-length effect.

Our previous work thoroughly investigated the advantages of different stiffness measurement methods for poly (vinyl alcohol) (PVA) hydrogels [47]. A reduced selection of compressive, rheological, and macroindentation experiments was investigated on the multi-arm PEG hydrogels in case they differed from the PVA hydrogel data (Supp. Fig. S2). The rheology confirmed for all formulations that there was a negligible viscous component compared to the elastic contribution within the linear viscoelastic range. Furthermore, preliminary cyclical compression studies on a subset of the PEG hydrogel formulations indicated negligible plastic deformation and full elastic recovery within the strain rates and ranges studied (data not shown). Like with PVA hydrogels, the compressive shear moduli were consistently higher than the rheological storage moduli, and the compression-macroindentation trend crossed over the line of equivalence trending towards compressive shear moduli being higher than macroindentation shear moduli at higher overall values. Since compressive shear modulus was established as a reliable indicator of PVA hydrogel stiffness in the previous work [47], it is used as the primary representation of measured stiffness for multi-arm PEG hydrogels in this study.

2.3. Structurally decoupled stiffness and solute transport in hydrogels

Structurally decoupling stiffness and solute transport in hydrogels without altering the hydrogel's chemical properties provides new opportunities for designing nuanced hydrogels for various applications, including drug delivery and encapsulation cell culture. Solute transport

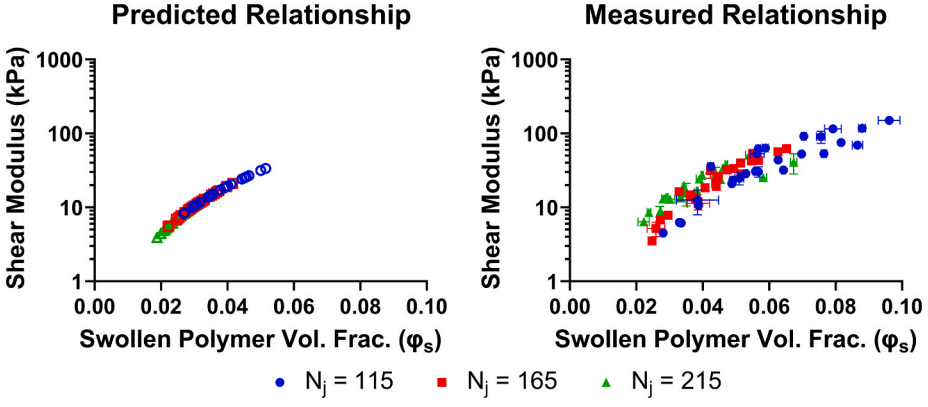

Fig. 2. Predicted and measured relationships between swollen polymer volume fraction (φ_s) and shear modulus (G). Error bars represent standard deviations ($n = 3$ for shear modulus and swelling measurements).

in each hydrogel formulation was measured by fluorescence recovery after photobleaching (FRAP) experiments with a small solute (fluorescein, 0.9 nm hydrodynamic radius) and a larger solute (20 kDa FITC-dextran, 2.9 nm) [35,37]. Diffusion coefficients for each hydrogel-solute pairing were calculated using our high-throughput modification of the Jönsson et al. spatial Hankel analysis program [37,50]. Since solute-independent metrics of transport in hydrogels, such as mesh size, do not provide broadly applicable summaries of their solute transport profiles [35], we use the diffusion coefficients of fluorescein and 20 kDa FITC-dextran in each hydrogel formulation as direct representations of their solute transport profiles. Mesh sizes are not directly discussed in this work because they are indirectly estimated structural parameters that neglect junction geometry effects on solute transport [37,46] and do not capture the nuances of how different solutes diffuse within the same hydrogel formulation [35,37]. Notably, solute transport within synthetic polymer hydrogels is dominated by diffusion [35,37], justifying FRAP-based self-diffusion coefficients as a summary of solute transport within the context of cells encapsulated within hydrogels, but within granular hydrogels [51], biopolymer hydrogels [52], and natural vascularized tissues capable of interstitial fluid flow [53], convection likely makes a significant contribution to solute transport. A critical comparison of solute transport in hydrogels and natural tissues will help to clarify the limitations of 3D hydrogel cell encapsulation for biomimetic cell culture environments.

Across the 73 multi-arm PEG hydrogel formulations, robust decoupling of stiffness and solute transport was achieved for both solutes, primarily driven by the degrees of polymerization between junctions (Fig. 3). The stiffness-diffusivity curves with fluorescein as the diffusing solute show a clear and consistent shift toward lower values in both stiffness and diffusivity with increasing degrees of polymerization between junctions. The larger 20 kDa FITC-dextran also shows increasing degrees of polymerization between junctions lowering both stiffness and solute diffusivity. While the fluorescein dataset showed comparable shifts between the three degrees of polymerization between junctions, the 20 kDa FITC-dextran dataset has the $N_j = 115$ group isolated but overlap for the two higher values, possibly suggesting a practical limit with diminishing diffusivity changes for further increases to N_j. The variations within the color N_j grouping are due to changes in the initial polymer volume fraction, junction functionality, and frequency of chain-end defects, which all have redundant effects of shifting formulations toward higher stiffness and lower solute diffusivity or vice versa. This indicates that the minimum requirement for decoupling stiffness and solute diffusivity in multi-arm PEG hydrogels is to simultaneously vary the degree of polymerization between junctions and one of the other three structural parameters.

Our previous efforts to decouple stiffness and solute transport in PVA hydrogels by varying the initial polymer volume fraction and degree of polymerization between junctions instead yielded a continuous curve (Supp. Fig. S3). The PVA stiffness-transport curve is comparable to previous results with PEG diacrylate (PEGDA) hydrogel formulations by other research groups, which also effectively varied the initial polymer volume fraction and degree of polymerization between junctions [29,30]. Comparison with these prior studies reinforces the novelty of the structural stiffness-transport decoupling in multi-arm PEG hydrogels. Additionally, the critical decoupling effect of the degree of polymerization between junctions is observed in multi-arm PEG hydrogels but not PVA or PEGDA hydrogels, possibly indicating that the highly homogeneous network structure of multi-arm PEG hydrogels [41] results in a different structure-property relationship than that of PVA and PEGDA hydrogels [36,45]. Specifically, PVA hydrogels are randomly crosslinked and therefore have a broad distribution of degrees of polymerization between junctions (N_j) unlike multi-arm PEG hydrogels, wherein N_j is set by the precursor macromer molecular weight. In PEGDA hydrogels, radical polymerization of acrylate end-groups produces kinetic chain junctions that vary stochastically in the number of attached PEG chains, whereas multi-arm PEG junction functionalities are set by the number of arms connected to each core. These differences make multi-arm PEG hydrogels a relatively ideal and controllable system. The multi-arm PEG-specific result of decoupling stiffness and solute transport via the degree of polymerization is not predicted by the swollen polymer network model and therefore requires further careful consideration and cross-evaluation with closely comparable hydrogel systems. Qualitatively, it is possible that the shorter chains are more strained (matching the increased stiffness) and therefore conformationally explore a smaller volume (consistent with statistical chain mechanics), leaving relatively larger void volumes for solutes to move through uninterrupted. High network homogeneity might explain why this differs from PVA hydrogels, but this hypothetical relationship should be further rigorously investigated.

2.4. Statistically evaluating stiffness and solute transport decoupling

To qualify the decoupling of stiffness and solute transport across hydrogel formulations, we developed a practical statistical definition of decoupling: one hydrogel formulation must have statistically significant differences (via *t*-test) in stiffness and non-significant differences in solute diffusivity with a second formulation in the dataset and statistically significant differences in solute diffusivity and non-significant differences in stiffness with a third formulation to qualify as decoupled. We applied that definition to iteratively filter our dataset until the remaining formulations were all statistically decoupled from each other. Since we are interested in hydrogel formulations that decouple stiffness and solute transport for both small solutes and large solutes, we also removed formulations that did not achieve decoupling for both fluorescein and 20 kDa FITC-dextran. The algorithm is provided as an R script in the supplementary materials.

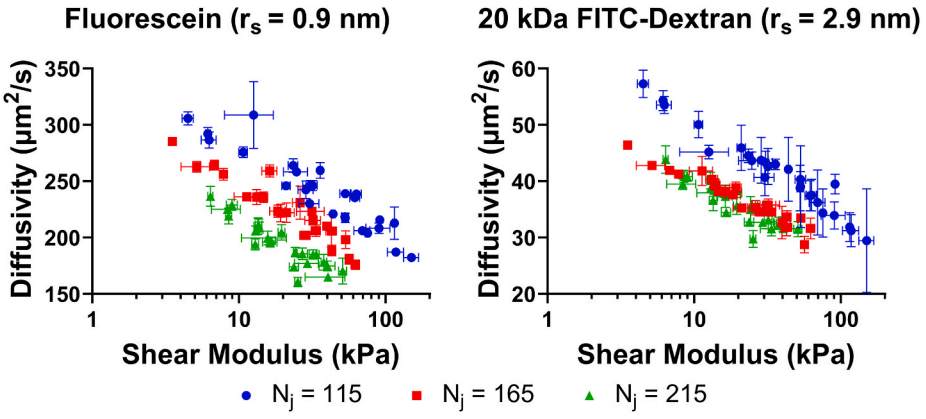

Fig. 3. Degree of polymerization between junctions (N_j) decouples stiffness and solute transport across the 73 multi-arm PEG hydrogel formulations studied. Increasing the degree of polymerization between junctions decreased shear modulus and decreased the diffusivity of both fluorescein and 20 kDa FITC-dextran within the hydrogels, whereas the other three structural parameters generally increased shear modulus when decreasing solute diffusivity. Error bars represent standard deviations ($n = 3$ for shear modulus measurements, $n = 9$ for diffusivity measurements). Free diffusion coefficients for fluorescein and 20 kDa FITC-dextran are $D_0 = 278\ \mu m^2/s$ and $D_0 = 85\ \mu m^2/s$, respectively [37].

The independent control variable for this statistical decoupling approach is the quantitative definition of statistically significant differences, typically $\alpha = 0.05$. That value is traditionally used to confirm statistically significant differences, whereas we are equally concerned with non-significant differences. Therefore, we increased the alpha value to reduce the likelihood of one hydrogel formulation having a stiffness or diffusivity that's non-significantly different from another hydrogel formulation's value. Fig. 4 shows how the number of decoupled formulations reduces as alpha increases, with 46 formulations remaining at $\alpha = 0.05$, 26 formulations at $\alpha = 0.20$, and only 12 formulations at $\alpha = 0.25$. Alpha values beyond 0.30 yielded no acceptable formulations.

The decoupled dataset has reduced property ranges compared to the overall, 73-formulation dataset. In the overall dataset, shear modulus ranged from 3.5 kPa to 150 kPa, diffusivity of fluorescein ranged from 160 $\mu m^2/s$ to 308 $\mu m^2/s$, and diffusivity of 20 kDa FITC-dextran ranged from 28.7 $\mu m^2/s$ to 57.3 $\mu m^2/s$. The 12-formulation, $\alpha = 0.25$ decoupled dataset had shear moduli from 21 kPa to 69 kPa, fluorescein diffusivities from 174 $\mu m^2/s$ to 260 $\mu m^2/s$, and 20 kDa FITC-dextran diffusivities from 31.6 $\mu m^2/s$ to 45.9 $\mu m^2/s$. The stiffness range of the decoupled dataset is 33% of the original dataset. Likewise, the reduced fluorescein diffusivity range is 58% of the original, and the 20 kDa FITC-dextran range is 50% of the original. Future exploration of structural parameter combinations (e.g., 8-arm hydrogels with lower initial polymer volume fractions than synthesized here) or improvements to structural control of hydrogel properties will enable decoupling over broader ranges of properties, ideally covering the ranges of properties found within both healthy and diseased biological tissues.

While the ranges for solute transport may seem small compared to the ranges for stiffness, it is important to note that stiffness is fully dependent on the polymer network, whereas solute transport is also heavily influenced by the properties of the solute. It is commonly assumed that smaller solutes would be less affected by the network structure since they are much smaller than the typical synthetic network's mesh size or even mesh radius, but the net change in diffusion coefficient for the small solute fluorescein is greater than the net change for the larger 20 kDa FITC-dextran, and the relative change is comparable between the two, suggesting that small molecule diffusivity is also greatly affected by network structure [35]. While in-hydrogel diffusion coefficients for the 20 kDa FITC-dextran are consistently below their free solute diffusion coefficients ($D_0 = 85\ \mu m^2/s$), some in-hydrogel diffusion coefficients for fluorescein exceed the free diffusion coefficient ($D_0 = 278\ \mu m^2/s$), suggesting a possible crossover point where the hydrogel formulation enhances transport for certain molecules. However, this conclusion requires further validation due to technical differences in how diffusion coefficients were measured in hydrogels and in free solution [37]. Overall, the ability of the hydrogel formulation to double the time it takes for a solute (small molecule or soluble protein) to reach an encapsulated cell could serve as a critical rate-limiting effect for many cellular processes, such as serum-dependent proliferation [54] or cytokine signaling [19].

From the 12 highly decoupled formulations, we extracted a set of four formulations that could be used to test how encapsulated cells respond to decoupled stiffness and solute transport in their environment

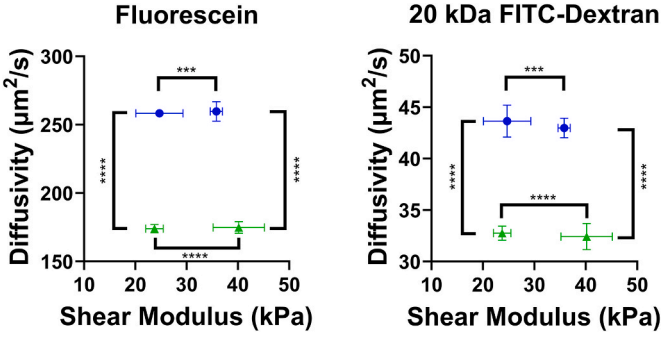

Fig. 5. Four formulations demonstrate the capacity to decouple stiffness and solute transport via hydrogel structural parameters. Each formulation has another formulation with equivalent solute diffusivity but significantly different shear modulus and a third formulation with equivalent shear modulus but significantly different solute diffusivity, across both a large and small solute (20 kDa FITC-dextran and fluorescein, respectively). Error bars represent standard deviations ($n = 3$ for shear modulus measurements, $n = 9$ for diffusivity measurements).

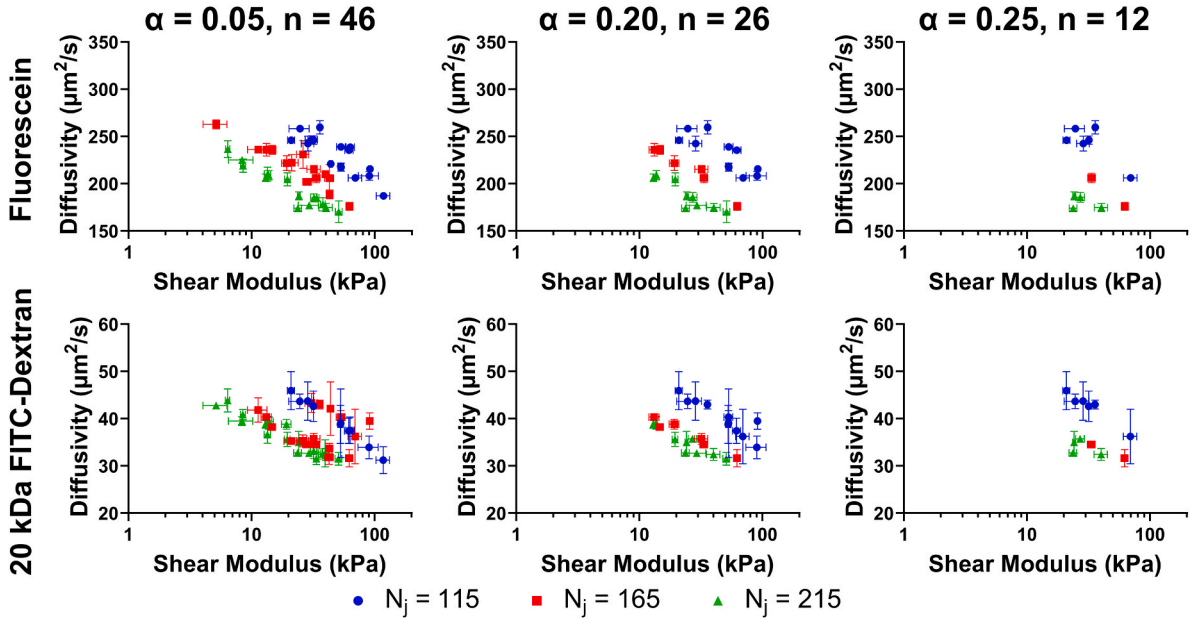

Fig. 4. Increasing the α-value of the statistical decoupling algorithm selects increasingly decoupled hydrogel formulations. The algorithm iteratively removes formulations that are not decoupled from other formulations in the dataset and confirms that the remaining formulations have statistically decoupled shear modulus and diffusivity for both fluorescein and 20 kDa FITC-dextran. $\alpha > 0.25$ results in no passing formulations. Error bars represent standard deviations ($n = 3$ for shear modulus measurements, $n = 9$ for diffusivity measurements).

(Fig. 5). There is a low-transport, low-stiffness formulation (A4-N215-V100-F00), a low-transport, high-stiffness formulation (A6-N215-V075-F00), a high-transport, low-stiffness formulation (A6-N115-V050-F02), and a high-transport, high-stiffness formulation (A4-N115-V050-F00). Notably, the final four formulations vary across all four structural parameters, justifying the simultaneous manipulation of all four parameters for achieving decoupling (i.e., only manipulating two or three parameters may require more extensive and precise tuning to reach the same set of properties). We hypothesize that cellular behaviors that are solute transport-dependent would differ between a stiffness-paired low-transport and high-transport formulation but not differ between a transport-paired low-stiffness and high-stiffness formulation. Stiffness-dependent cell behaviors would have the opposite response, and behaviors that respond to both stiffness and solute transport could be further evaluated by comparing the diagonal formulations (e.g., low-transport and low-stiffness vs. high-transport and high-stiffness). Together, these biocompatible, property-decoupled multi-arm PEG hydrogel formulations will help to clarify mechanisms of cell-environment interactions.

2.5. The swollen polymer network model predicts structure-property correlations in hydrogels

Swelling, stiffness, and solute diffusivity were predicted for each hydrogel formulation using the swollen polymer network model. Comparing measured and modeled properties, including how each of the structural parameters affects those properties, provides opportunities to improve the accuracy of the fundamental model by testing assumptions and comparing alternative modeling approaches. These evidence-based checks on the model will then be applied when making new hydrogels, improving property-oriented hydrogel design for many biomedical applications.

We first compared measured swelling, stiffness, and solute transport properties to predicted values to evaluate the overall correlations between predictions and measurements (Fig. 6). Notably, swelling has a precise, linear prediction-measurement correlation over all 73 hydrogel formulations, but the prediction underestimates the measured range of swollen polymer volume fractions. Stiffness also has a precise correlation over two orders of magnitude. The measurement-prediction correlations for solute diffusivity are discussed in greater detail in our previous work [35]. Contrary to the predictions, increasing the degree of polymerization between junctions reduced diffusion coefficients for both fluorescein and 20 kDa FITC-dextran. Furthermore, predictions overestimated the influence of junction functionality on the diffusion coefficient of the larger 20 kDa FITC-dextran solute, as indicated by the horizontally separated series (Figs. 6 and 20 KDA FITC-Dextran).

Table 1 summarizes measured structure-property correlations and identifies whether those correlations match predictions. Increasing initial polymer volume fraction and junction functionality increased swollen polymer volume fraction and shear modulus and decreased solute diffusion coefficients. Increasing the frequency of chain-end defects decreased swollen polymer volume fraction and shear modulus and increased solute diffusion coefficients. Increasing the degree of polymerization between junctions decreased all three properties. All measured trends match predictions (shared a positive or negative structure-property correlation) except for the degree of polymerization between junctions and solute diffusion coefficient, which was predicted to be a positive correlation. With the previously studied PVA hydrogels, increasing the degree of polymerization between junctions increased the solute diffusion coefficients as predicted (Supp. Fig. S3). These results suggest that the swollen polymer network model accurately captures the modeled structure-property correlations except for a unique interaction between the degree of polymerization between junctions and solute transport observed in multi-arm PEG hydrogels. Developing a mechanistic explanation for this interaction would require further investigation with similar hydrogel systems.

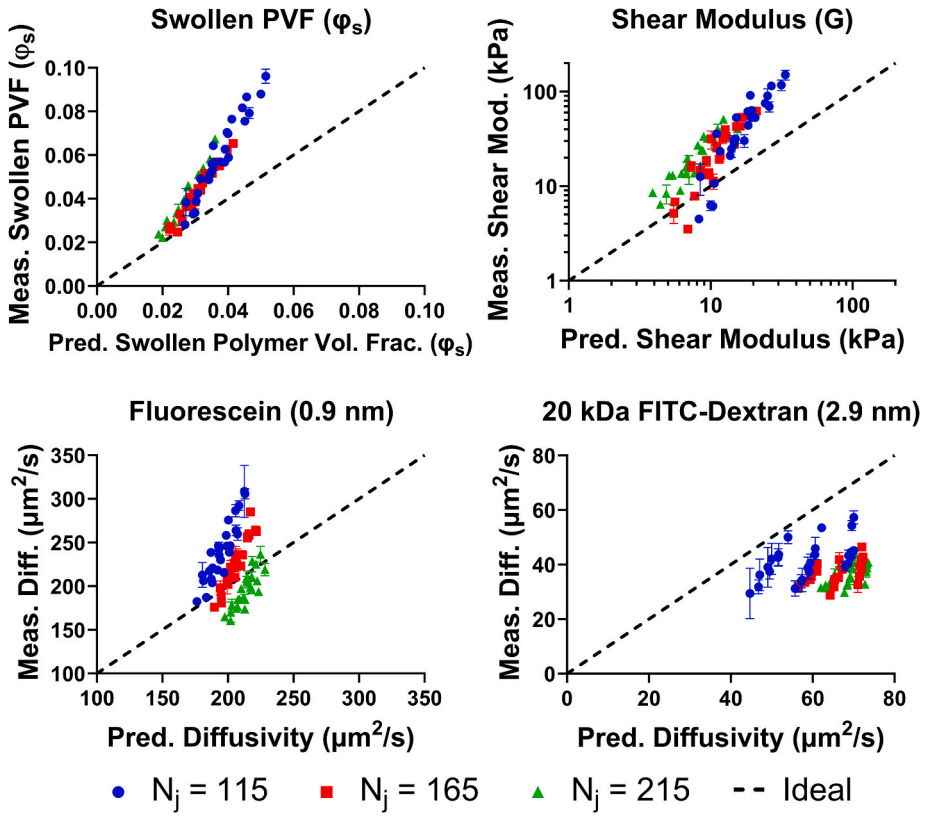

Fig. 6. Correlations between predicted properties and measured properties. Predictions were made using the swollen polymer network model. Error bars represent standard deviations ($n = 3$ for shear modulus and swelling measurements, $n = 9$ for diffusivity measurements).

Table 1
Structure-property correlations and measurement-prediction trends.

Structural Parameters	Measured Correlations			Model Accuracy for Structure-Property Trends		
	Swollen PVF (φ_s)	Shear Modulus (G)	Diffusivity (D)	Swollen PVF (φ_s)	Shear Modulus (G)	Diffusivity (D)
Initial Polymer Vol. Frac. (φ_0)	+	+	−	✓	✓	✓
Junction Functionality (f)	+	+	−	✓	✓	✓
Degree of Polym. Between Jun. (N_j)	−	−	−	✓	✓	✗
Freq. of Chain-End Defects (γ)	−	−	+	✓	✓	✓

"+" indicates a positive measured correlation between the structural parameter and network property. "-" indicates a negative measured correlation between the structural parameter and network property. "✓" indicates that the direction of the predicted correlation matches the direction of the measured correlation (positive or negative), "✗" indicates that the direction of the predicted correlation does not match the direction of the measured correlation.

2.6. Improving hydrogel modeling with diverse hydrogel formulations

The swollen polymer network is intended to be a general model for structurally designing hydrogels to produce desired physical properties, simultaneously addressing swelling, stiffness, and solute transport. The swollen polymer network model was initially assembled from fundamental theories linking hydrogel structure to the three properties [46]. We then tested structure-swelling correlations on PVA hydrogels, PEGDA hydrogels, and gelatin methacrylate (GelMA) hydrogels and found that the swelling predictions were accurate for synthetic hydrogels (PVA and PEGDA) but not the biopolymer GelMA, likely due to higher order coiling interactions affecting the GelMA network structure [45]. Further consideration of network geometry based on these results led us to propose the mesh radius amendment to the solute transport component of the swollen polymer network model [36]. Then, stiffness and solute transport measurements in PVA hydrogels indicated that controlling the initial polymer volume fraction and degree of polymerization between junctions was not sufficient to decouple stiffness and solute transport (Supp. Fig. S3) [37,47]. We then investigated two additional structural parameters, junction functionality and the frequency of chain-end defects, using multi-arm PEG hydrogels, which validated our hypothesis that network geometry influences the transport of solutes within a hydrogel [35]. In this final, summative study, we compared solute diffusion and stiffness in the four-parameter library of multi-arm PEG hydrogels, demonstrating that the four structural parameters enables robustly decoupled control of stiffness and solute transport. Together, this work provides evidence that iteratively testing the assumptions of a fundamentally derived structure-property model with a diverse library of hydrogel formulations leads to validated model improvements that increasingly capture nuanced hydrogel properties.

Several intersectional insights from this series of experiments warrant reporting but require the context of the swollen polymer network model and its utility in designing hydrogels with desirable properties. Here, we address results on the propagation of error through the swollen polymer network model, the comparison of phantom and affine modeling assumptions, the idea of a reference ratio introduced in our previous work on hydrogel swelling [45], and the use of a second-order polymer-solvent interaction parameter (χ_2) to describe PEG hydrogel swelling.

The swollen polymer network model fundamentally predicts swelling, stiffness, and solute transport based on structural parameters [36,46], but the swollen polymer volume fraction is calculated first using the equilibrium swelling equation and then used in the calculations for shear modulus and solute diffusion coefficients. Therefore, any errors associated with the equilibrium swelling calculation propagate into the other property predictions. Directly measuring the swollen polymer volume fraction and then using the measured value in shear modulus and diffusion coefficient calculations removes the error propagation effect. We compared how using the predicted or measured swollen polymer volume fraction influences the correlation between predicted and measured shear moduli, finding only a small shift in the overall correlation (Supp. Fig. S4). This internal comparison qualifies the validity of the swollen polymer network model.

Phantom and affine molecular deformation models are both commonly used to describe the structure-property relationships of swollen polymer networks [46,49,55–57]. Briefly, the affine model assumes that junctions move proportionally to bulk deformations, and the phantom model removes that assumption [46]. Since the affine model is associated with entanglements restraining network junction mobility [58], the phantom model has been increasingly applied to hydrogels made in solution with a low frequency of polymer entanglements [46,49,59]. Mathematically, the difference between the models depends on the network's junction functionality (the phantom model adds a term of $1-\frac{2}{f}$) [46]. By controlling junction functionality in our multi-arm PEG hydrogels, we capture the difference between phantom-based predictions and affine-based predictions of swelling and stiffness. For both swelling and stiffness, the phantom-based predictions were more precisely associated with measurements than the affine-based predictions, i.e. less spread due to the changing junction functionalities (Supp. Fig. S5). The difference in measurement-prediction correlation indicates that the phantom-based version of the swollen polymer network is more appropriate for the dilute hydrogels studied here ($\varphi_0 \leq 0.10$), especially when varying their junction functionalities.

In a previous publication, we introduced the reference ratio as a characteristic property of hydrogels that describes the extent of hydrogel swelling from their initial state to the equilibrium swollen state [45]. In that work, we found independent correlations for PVA hydrogels and PEGDA hydrogels between 1) initial polymer volume fraction and relaxed polymer volume fraction and 2) degree of polymerization between junctions and the reference ratio. In this study, we found that multi-arm PEG hydrogels did have a positive correlation between initial polymer volume fraction and relaxed polymer volume fraction, but it was not as precise as PVA hydrogels or PEGDA hydrogels (Supp. Fig. S6). Moreover, the strong linear correlation between the degree of polymerization between junctions and the reference ratio was not observed for multi-arm PEG hydrogels (Supp. Fig. S6). We expected some differences between the multi-arm PEG dataset and the PVA and PEGDA datasets since the PVA and PEGDA hydrogels did not include variation along the junction functionality and frequency of chain-end defects structural axes, but with multi-arm PEG hydrogels, even initial polymer volume fraction has a distinct influence on the reference ratio, contrasting the independent correlations previously observed and undermining the importance of the reference ratio as a characteristic property. It is unclear whether the multi-arm PEG hydrogels differ because they are a more ideal model network with less heterogeneity than PVA hydrogels and PEGDA hydrogels [41,60], if their different crosslinking mechanisms create a different relationship between the initial and equilibrium-swollen polymer volume fractions, or if some other unconsidered influence is having a strong effect.

The polymer-solvent interaction parameter is associated with the miscibility of a specific polymer-and-solvent pairing [46,61]. It is typically summarized as a single, first-order parameter (χ_1) for practicality and brevity, but it can be expanded serially to represent a concentration-dependent relationship [46]. Furthermore, it is unclear whether the strains placed on a polymer in a network affect its miscibility with a solvent, potentially changing it from what is observed for a non-networked polymer. In the swollen polymer network model, increasing χ_1 increases the predicted swollen polymer volume fraction for all hydrogel formulations using that polymer. Increasing χ_2, the second-order polymer-solvent interaction parameter, increases the influence of structural parameters on the predicted swollen polymer volume fraction [62]. Increasing χ_2 from 0 to 0.8 for multi-arm PEG hydrogels increases the predicted swollen polymer volume fraction for dense hydrogel formulations but not dilute hydrogel formulations, improving the accuracy of the prediction-measurement correlation (Supp. Fig. S5A). However, further increasing χ_2 to 1.0 and 1.2 made it impossible to predict the swollen polymer volume fraction (Supp. Fig. S5A). Effectively, the equilibrium swelling equation calculation loses stability when the overall polymer-solvent interaction parameter becomes greater than 0.5 (indicating that polymer and solvent are no longer attracted to each other), which can occur for a combination of high swollen polymer volume fraction and high second-order polymer-solvent interaction parameter (Supp. Fig. S5B). Therefore, introducing a second-order polymer-solvent interaction parameter facilitates instability in the overall equilibrium swelling calculation.

Because the polymer-solvent interaction parameter is applicable if the dominant polymer is consistent, prior data from PEGDA hydrogels can validate the use of the second-order polymer-solvent interaction parameter for multi-arm PEG hydrogels. For the PEGDA hydrogels, increasing χ_2 to 0.6 improved the measurement-prediction correlation, and further increasing to 0.8 introduced the stability limit (Supp. Fig. S5C). Together with the multi-arm PEG data, these results indicate that using $\chi_1 = 0.426$ and $\chi_2 = 0.6$ may be appropriate for increasing the accuracy of swelling predictions for PEG-based hydrogels. This result may either be a refinement of the polymer-solvent interaction parameter that was neglected or overly generalized when the application focus was simpler non-network polymer-solvent systems or it could be an observation specific to networked PEGs in water. Since swelling is a key component of property predictions for hydrogels, the higher-order polymer-solvent interaction parameters for common hydrogel polymers should be further investigated and cross-validated.

2.7. Physical properties relevance to hydrogel-encapsulated cells

Control of microenvironmental stiffness and solute transport is relevant to the behavior of hydrogel-encapsulated cells. 3D hydrogel encapsulation of cells is increasingly used as an *in vitro* model to mimic and control key functional aspects of different tissues and relevant microenvironments, including tumors and stem cell niches [1,21,63]. Cellular mechanosensing of the stiffness of 2D and 3D hydrogel microenvironments is well-established [64], with effects on cell proliferation [12,65], differentiation [7,8,66], and drug resistance [67–69], and has pushed the field to consistently incorporate integrin-binding peptides and other mechano-active components into cell-encapsulating hydrogels [42,70–73]. However, control and assessment of how solute transport affects cells encapsulated in hydrogels are less established, likely because solute transport is limited in 3D encapsulation but not 2D substrate culture and because solute transport in hydrogels is more challenging to characterize than stiffness [35,37,47]. Hydrogel-mediated transport of soluble proteins affects stem cell differentiation by regulating the balance between paracrine and autocrine signaling that cells experience [19,74]. Other areas poised for disruptive investigations of cellular responses to environmentally regulated solute transport include drug delivery to cells within dense ECM and the serum deprivation-dependent dormancy of cancer cells [54,75]. By decoupling stiffness and solute transport within hydrogels, we gain the opportunity to identify situations where control of solute transport has a strong effect on cell behavior without confounding effects from simultaneously changing stiffness. Likewise, we can reduce the risk of claiming stiffness is the driver of cell responses to changing microenvironments when other property changes may be causing the differences in cell behaviors.

The structural decoupling of hydrogel properties is likely limited to synthetic polymer hydrogels and therefore less relevant to biopolymer hydrogels commonly used for cell encapsulation. Generally, biopolymer hydrogels have more complex structures that increase polymer rigidity compared to synthetic polymer hydrogels, creating void spaces within the hydrogels that are several orders of magnitude larger than synthetic polymer mesh radius portals and therefore dramatically less restrictive to solute transport [45,46,76,77].

Finally, while multi-arm PEGs are used in many hydrogel encapsulation cell culture systems [40,42,43,70,73], several modifications to the current study are needed to produce cell-relevant hydrogel formulations for studying how decoupled stiffness and solute transport affect cell behaviors. First, formulations with lower stiffnesses than those produced here are needed to match the stiffness of common tissues studied with hydrogels, including brain tissue and bone marrow [78,79]. Creating hydrogels with different solute transport profiles at tissue-relevant stiffnesses without failing gelation is a technical challenge that can use the structural principles established here but is beyond the scope of this proof-of-concept study. Second, these hydrogels will need to incorporate integrin-binding peptides, which can be achieved by using the unreacted end-groups left over by non-zero frequencies of chain-end defects. MMP-degradable peptides can be substituted for non-degradable crosslinkers to enable cell-driven degradation and promote cell mobility over time. Third, it would be helpful to use radical-free gelation chemistry to minimize the effects of radical oxygen species (ROS) on cells during the encapsulating gelation process [80–83]. Differences in ROS generation based on the conditions needed to complete gelation could overshadow cell responses to the stiffness or solute transport profile of their environment. Addressing these considerations alongside structurally decoupled stiffness and solute transport will unlock new avenues for studying how cells interact with their physical environment.

3. Conclusions

Creating a library of 73 multi-arm PEG hydrogel formulations with simultaneous variation in four structural parameters overcame a critical obstacle in biomimetic hydrogel design: decoupling stiffness and solute transport. Because this approach emphasizes the network structure instead of specific chemical interactions, it may be broadly applicable to hydrogels made from many types of polymers. The swollen polymer network model helped to identify the four independent structural parameters of interest and predict their influences on hydrogel physical properties, but the model did not fully predict the relationships between structure and property, notably mispredicting the relationship between the degree of polymerization between junctions and solute diffusivity. However, the same relationship was previously correctly predicted in PVA hydrogels, suggesting the possibility of a polymer-specific or crosslinking method-specific interaction. Finally, the dataset of physical properties associated with each multi-arm PEG hydrogel formulation further refined the swollen polymer network model by testing assumptions, especially those associated with the junction functionality structural parameter, which is otherwise under-investigated. Decoupled stiffness and solute transport in hydrogels will help to distinguish how cells react to stiffness and transport-dependent environmental stimuli when encapsulated in 3D hydrogels.

4. Experimental Section

Norbornene functionalization of multi-arm PEG: Multi-arm PEG precursor molecules were end-functionalized with norbornene as

previously described [35]. Briefly, nine precursor polymers were used (JenKem Technology; Plano, TX): (1) 4-arm, 10 kDa PEG, (2) 4-arm, 15 kDa, (3) 4-arm, 20 kDa, (4) 6-arm, 15 kDa, (5) 6-arm, 21 kDa, (6) 6-arm, 30 kDa, (7) 8-arm, 20 kDa, (8), 8-arm, 30 kDa, and (9) 8-arm, 40 kDa. The nine polymers were chosen to explore three junction functionalities (4, 6, and 8) and three sets of chain-arm lengths (approx. 2.5 kDa per arm, 3.75 kDa, and 5 kDa), which correspond to the degree of polymerization between junctions ($N_j = 115, 165, 215$). For all precursor macromers, polydispersity was confirmed by the manufacturer to be less than 1.05 and independently confirmed upon receipt by gel permeation chromatography (data available upon request). All other reagents and solvents were purchased from Sigma-Aldrich (St. Louis, MO) unless otherwise noted. All reagent concentrations were scaled to the expected concentration of hydroxyl end-groups for 5 g of the batch's PEG precursor. Initially, 5 molar equivalents (to PEG –OH groups) of N, N′-dicyclohexylcarbodiimide and 10 molar equivalents of 5-norbornene-2-carboxylic acid were mixed in 20 mL of dichloromethane under a nitrogen atmosphere and reacted at room temperature for 30 min. The product solution was then centrifuged at 3000 rpm for 10 min at room temperature to separate the precipitated byproduct. The subnatant liquid was then added to a 40 mL dichloromethane solution on ice that contained 5 g of multi-arm PEG precursor, 5 molar equivalents of pyridine, and 0.5 molar equivalents of 4-(dimethylamino)pyridine (DMAP). The resulting solution was left to react overnight. The reacted solution was precipitated and centrifuged twice in ice-cold diethyl ether, then dried. The dry pellet was then resuspended in deionized water and dialyzed for 24 h (2000 MWCO) before lyophilization and storage until use. Norbornene functionalization was confirmed via 1H NMR (Agilent MN400) in triplicate [84].

Multi-arm PEG hydrogel synthesis: Multi-arm PEG hydrogels were synthesized as described previously [35]. Briefly, 73 intact hydrogel formulations were made by simultaneously varying four structural parameters. The structure of the multi-arm precursors defined the degree of polymerization between junctions ($N_j = 115, 165, 215$) and the junction functionality ($f = 4,6,8$). The concentration of the polymer in water defined the initial polymer volume fraction ($\varphi_0 = 0.050, 0.075, 0.100$), and the stoichiometric ratio of norbornene groups to cross-linking thiols (dithiothreitol, DTT) defined the frequency of chain-end defects ($\gamma = 0, 0.2, 0.4$).

Hydrogel swelling characterization: Volumetric swelling was measured via the buoyancy-based method as described previously [45]. Briefly, hydrogel volumes were measured immediately after synthesis, after swelling to equilibrium, and after complete drying. Relaxed polymer volume fractions were calculated by dividing the dry volume by the relaxed volume. Swollen polymer volume fractions were calculated by dividing the dry volume by the swollen volume. The reference ratio was calculated by dividing the swollen volume by the relaxed volume. Three samples were used per hydrogel formulation for swelling measurements. Raw data are provided in the supplementary materials.

Hydrogel stiffness measurements: The stiffness of each multi-arm PEG hydrogel formulation swelling equilibrium was measured in three ways, using the compression, rheology, and macroindentation methods described previously [47]. Briefly, the shear modulus was calculated from compression experiments by fitting the compressive stress and strain of the samples over 10–20% strain to a Neo-Hookean hyperelastic model. Storage modulus for each hydrogel was measured via a rheometer over 0.01–1% strain and a frequency of 1 Hz. Multi-arm PEG hydrogels were found to be effectively elastic (data not shown), justifying the use of storage modulus as an approximate representation of shear modulus. Macroindentation was measured with 10% indentation of a 3 mm diameter spherical probe and fit to a Hertz model to calculate the shear modulus. Three samples were used per hydrogel formulation for all stiffness measurements. Raw data are provided in the supplementary materials.

Solute diffusivity in hydrogels: Solute diffusivities in multi-arm PEG hydrogels were measured at swelling equilibrium via FRAP experiments as described previously [35]. Briefly, samples of each hydrogel formulation were incubated for 24 h in a 10 μM solution of fluorescein or 20 kDa FITC-dextran in PBS. Solute free diffusion coefficients (D_0) were determined via FRAP in solution experiments, and hydrodynamic radii (r_s) were calculated using the Stokes-Einstein equation, yielding 0.9 nm hydrodynamic radius for fluorescein and 2.9 nm for 20 kDa FITC-dextran. FRAP experiments were performed with three runs per sample ($n = 9$ per solute-formulation pairing) on a Zeiss LSM710 Confocal Microscope (Zeiss, Germany). FRAP analysis was performed using our high-throughput FRAP analysis MATLAB program [37], yielding diffusion coefficients for each solute-hydrogel pairing. Raw data are provided in the supplementary materials.

Predictive modeling of hydrogel properties: The swollen polymer network model was used to make *a priori* predictions of each hydrogel formulation's swollen polymer volume fraction, shear modulus, and solute diffusion coefficients [35–37,45–47]. Raw prediction data are provided in the supplementary materials. Swollen polymer volume fractions (φ_s) were calculated via Equation (1).

$$\varphi_s^{-\frac{1}{3}}\left[\ln(1-\varphi_s)+\varphi_s+\chi_1\varphi_s^2\right] = -1 * \frac{\rho_d V_1}{M_r N_j}(1-\gamma)\left(1-\frac{2}{f}\right)\varphi_0^{\frac{2}{3}} \tag{1}$$

in Equation (1), N_j, γ, f, and φ_0 are defined by the specific hydrogel formulation's network structure as explained above, and $\chi_1 = 0.426$ for PEG and water, $\rho_d = 1.12\, g/mL$ is the dry density for PEG, $V_1 = 18\, mL/mol$ for water, and $M_r = 44\, g/mol$ is the repeating unit formula weight for PEG [45].

Shear moduli (G) were calculated via Equation (2), using the swollen polymer volume fractions from Equation (1).

$$G = \frac{RT\rho_d}{M_r N_j}(1-\gamma)\left(1-\frac{2}{f}\right)\varphi_0^{\frac{2}{3}}\varphi_s^{\frac{1}{3}} \tag{2}$$

in Equation (2), $R = 8314\,\frac{\text{kPa mL}}{\text{mol K}}$ is the ideal gas constant and $T = 298\, K$ is the temperature of the system [45]. Other parameters are defined below Equation (1).

Solute diffusion coefficients in hydrogels (D) were calculated using Equations (3)–(5) [35,85,86].

$$\xi = \varphi_s^{-\frac{1}{3}}\left(\left(1-\frac{2}{f}\right)\bar{l}^2 C_\infty \lambda N_j\right)^{\frac{1}{2}} \tag{3}$$

in Equation (3), ξ is the mesh size, $\bar{l} = 0.15\, nm$, $C_\infty = 4$, and $\lambda = 3$ for PEG [45,87].

$$r_m = \begin{cases} \frac{\sqrt{6}}{3}\xi & f = 4 \\ \frac{1}{2}\xi & f = 6 \\ \frac{\sqrt{2}}{4}\xi & f = 8 \end{cases} \tag{4}$$

in Equation (4), r_m is the mesh radius, dependent on the mesh size and the junction functionality (f) of the network. The relationship between mesh radius and mesh size is only known for regular polyhedron crystal structures that can be perfectly tessellated in 3D [36].

$$\frac{D}{D_0} = \text{erf}\left(\frac{r_{FVW}}{r_s}\right)\exp\left[-1 * \left(\frac{r_s}{r_{FVW}}\right)^3\left(\frac{\varphi_s}{1-\varphi_s}\right)\right] + \text{erfc}\left(\frac{r_{FVW}}{r_s}\right)\exp\left[-\frac{\pi}{4}\left(\frac{r_s+r_f}{r_m}\right)^2\right] \tag{5}$$

in Equation (5), D_0 is the diffusivity of the solute in a free aqueous solution and r_s is the associated hydrodynamic radius of the solute. As measured previously [37], for fluorescein, $D_0 = 278\, \mu m^2/s$ and $r_s = 0.88\, nm$. For 20 kDa FITC-dextran, $D_0 = 85\, \mu m^2/s$ and $r_s = 2.89\, nm$.

The average radius of free volume voids in water is $r_{FVW} = 0.269\,nm$ [86], and the fiber radius of PEG with a monolayer of water is $r_f = 0.51\,nm$.

Statistical analysis of stiffness-diffusivity decoupling: Statistical evaluation of stiffness-diffusivity decoupling was performed using a custom R script. Within the available set of multi-arm PEG hydrogel formulations, we defined decoupling as one hydrogel formulation having non-significant differences in stiffness (compressive, via *t*-test) and significant differences in solute diffusivity with a second hydrogel formulation as well as non-significant differences in solute diffusivity and significant differences in stiffness with a third hydrogel formulation, all within the dataset. Since solute diffusivity was defined by both the fluorescein and 20 kDa FITC-dextran diffusivity, each formulation had to meet the significance criteria for both solutes. Significance was determined by the choice of alpha values for the *t*-test, with a higher alpha value raising the required similarity between values for non-significant differences. We applied this definition iteratively to the dataset, removing hydrogel formulations that did not meet the criteria each round until further iterations no reduced the dataset for a given alpha value. The R script used for this analysis is provided in the supplementary materials.

CRediT authorship contribution statement

Nathan R. Richbourg: Conceptualization, Methodology, Software, Validation, Formal analysis, Investigation, Resources, Data curation, Writing – original draft, Writing – review & editing, Visualization, Project administration, Funding acquisition. **Nicholas A. Peppas:** Conceptualization, Resources, Supervision, Funding acquisition.

Declaration of competing interest

The authors declare that they have no known competing financial interests or personal relationships that could have appeared to influence the work reported in this paper.

Data availability

All data for this paper is available online, links provided in SI.

Acknowledgments

The support for this work was provided by the National Science Foundation (1610403 for N. R. R.) and the National Institutes of Health (EB022025, GM043337 for N. A. P.). N. A. P. is further supported by the Cockrell Family Regents Chair in Engineering for the Institute of Biomaterials, Drug Delivery, and Regenerative Medicine and the UT-Portugal Collaborative Research Program. N. R. R. is further supported by the Cockrell Graduate Continuing Fellowship. We thank Professor Nathaniel Lynd and Benjamin Pedretti at UT Austin for performing GPC to confirm the molecular weight and dispersity of our multi-arm PEG precursors as well as Garrett Blake and the UT Austin NMR core facility for training and support on ^{1}H NMR studies.

Appendix A. Supplementary data

Supplementary data to this article can be found online at https://doi.org/10.1016/j.biomaterials.2023.122272.

References

[1] S.R. Caliari, J.A. Burdick, A practical guide to hydrogels for cell culture, Nat. Methods 13 (2016) 405–414.
[2] K.L. Wiley, B.P. Sutherland, B.A. Ogunnaike, A.M. Kloxin, Rational design of hydrogel networks with dynamic mechanical properties to mimic matrix remodeling, Adv. Healthcare Mater. 11 (7) (2022), 2101947.
[3] H. Kim, A. Wirasaputra, F. Mohammadi, A.N. Kundu, J.A.E. Esteves, L.M. Heiser, A. S. Meyer, S.R. Peyton, Live cell lineage tracing of dormant cancer cells, Adv. Healthcare Mater. (2023), 2202275 n/a(n/a).
[4] T.P. Kraehenbuehl, P. Zammaretti, A.J. Van der Vlies, R.G. Schoenmakers, M. P. Lutolf, M.E. Jaconi, J.A. Hubbell, Three-dimensional extracellular matrix-directed cardioprogenitor differentiation: systematic modulation of a synthetic cell-responsive PEG-hydrogel, Biomaterials 29 (18) (2008) 2757–2766.
[5] O.Y. Dudaryeva, A. Bucciarelli, G. Bovone, F. Huwyler, S. Jaydev, N. Broguiere, M. al-Bayati, M. Lütolf, M.W. Tibbitt, 3D confinement regulates cell life and death, Adv. Funct. Mater. (2021), 2104098.
[6] J. Baek, P.A. Lopez, S. Lee, T.-S. Kim, S. Kumar, D.V. Schaffer, Egr1 is a 3D matrix–specific mediator of mechanosensitive stem cell lineage commitment, Sci. Adv. 8 (15) (2022), eabm4646.
[7] A.J. Engler, S. Sen, H.L. Sweeney, D.E. Discher, Matrix elasticity directs stem cell lineage specification, Cell 126 (4) (2006) 677–689.
[8] D.E. Discher, P. Janmey, W. Yu-li, Tissue cells feel and respond to the stiffness of their substrate, Science 310 (5751) (2005) 1139–1143.
[9] J. Yang, Y. Li, Y. Liu, D. Li, L. Zhang, Q. Wang, Y. Xiao, X. Zhang, Influence of hydrogel network microstructures on mesenchymal stem cell chondrogenesis in vitro and in vivo, Acta Biomater. 91 (2019) 159–172.
[10] S.R. Peyton, Z.I. Kalcioglu, J.C. Cohen, A.P. Runkle, K.J. Van Vliet, D. A. Lauffenburger, L.G. Griffith, Marrow-Derived stem cell motility in 3D synthetic scaffold is governed by geometry along with adhesivity and stiffness, Biotechnol. Bioeng. 108 (5) (2011) 1181–1193.
[11] E. Hui, J.L. Sumey, S.R. Caliari, Click-functionalized Hydrogel Design for Mechanobiology Investigations, Molecular Systems Design & Engineering, 2021.
[12] O. Chaudhuri, J. Cooper-White, P.A. Janmey, D.J. Mooney, V.B. Shenoy, Effects of extracellular matrix viscoelasticity on cellular behaviour, Nature 584 (7822) (2020) 535–546.
[13] Y. Liang, J. Jeong, R.J. DeVolder, C. Cha, F. Wang, Y.W. Tong, H. Kong, A cell-instructive hydrogel to regulate malignancy of 3D tumor spheroids with matrix rigidity, Biomaterials 32 (35) (2011) 9308–9315.
[14] J.S. Choi, B.A.C. Harley, The combined influence of substrate elasticity and ligand density on the viability and biophysical properties of hematopoietic stem and progenitor cells, Biomaterials 33 (18) (2012) 4460–4468.
[15] J. Prager, C.F. Adams, A.M. Delaney, G. Chanoit, J.F. Tarlton, L.-F. Wong, D. M. Chari, N. Granger, Stiffness-matched biomaterial implants for cell delivery: clinical, intraoperative ultrasound elastography provides a 'target' stiffness for hydrogel synthesis in spinal cord injury, J. Tissue Eng. 11 (2020), 2041731420934806.
[16] Y. Cao, B.H. Lee, H.B. Peled, S.S. Venkatraman, Synthesis of stiffness-tunable and cell-responsive Gelatin–poly(ethylene glycol) hydrogel for three-dimensional cell encapsulation, J. Biomed. Mater. Res. 104 (10) (2016) 2401–2411.
[17] K. Adebowale, Z. Gong, J.C. Hou, K.M. Wisdom, D. Garbett, H.-p. Lee, S. Nam, T. Meyer, D.J. Odde, V.B. Shenoy, O. Chaudhuri, Enhanced substrate stress relaxation promotes filopodia-mediated cell migration, Nat. Mater. 20 (2021) 1290–1299.
[18] E. Axpe, G. Orive, K. Franze, E.A. Appel, Towards brain-tissue-like biomaterials, Nat. Commun. 11 (1) (2020) 3423.
[19] B.P. Mahadik, N.A.K. Bharadwaj, R.H. Ewoldt, B.A.C. Harley, Regulating dynamic signaling between hematopoietic stem cells and niche cells via a hydrogel matrix, Biomaterials 125 (2017) 54–64.
[20] A.S. Caldwell, B.A. Aguado, K.S. Anseth, Designing Microgels for Cell Culture and Controlled Assembly of Tissue Microenvironments, Adv Funct Mater n/a, 2019, 1907670 n/a.
[21] A.E. Gilchrist, B.A.C. Harley, Engineered tissue models to replicate dynamic interactions within the hematopoietic stem cell niche, Adv. Healthcare Mater. (2021), 2102130 n/a(n/a).
[22] A.E. Gilchrist, S. Lee, Y. Hu, B.A.C. Harley, Soluble signals and remodeling in a synthetic gelatin-based hematopoietic stem cell niche, Adv. Healthcare Mater. 8 (2019), 1900751.
[23] L. Bian, C. Hou, E. Tous, R. Rai, R.L. Mauck, J.A. Burdick, The influence of hyaluronic acid hydrogel crosslinking density and macromolecular diffusivity on human MSC chondrogenesis and hypertrophy, Biomaterials 34 (2) (2013) 413–421.
[24] C. Cha, J.H. Jeong, J. Shim, H. Kong, Tuning the dependency between stiffness and permeability of a cell encapsulating hydrogel with hydrophilic pendant chains, Acta Biomater. 7 (10) (2011) 3719–3728.
[25] C. Cha, S.Y. Kim, L. Cao, H. Kong, Decoupled control of stiffness and permeability with a cell-encapsulating poly(ethylene glycol) dimethacrylate hydrogel, Biomaterials 31 (18) (2010) 4864–4871.
[26] S. Pedron, A.M. Pritchard, G.A. Vincil, B. Andrade, S.C. Zimmerman, B.A.C. Harley, Patterning three-dimensional hydrogel microenvironments using hyperbranched polyglycerols for independent control of mesh size and stiffness, Biomacromolecules 18 (4) (2017) 1393–1400.
[27] M.K. Lee, M.H. Rich, K. Baek, J. Lee, H. Kong, Bioinspired tuning of hydrogel permeability-rigidity dependency for 3D cell culture, Sci. Rep. 5 (1) (2015) 8948.
[28] N. Lorén, J. Hagman, J.K. Jonasson, H. Deschout, D. Bernin, F. Cella-Zanacchi, A. Diaspro, J.G. McNally, M. Ameloot, N. Smisdom, M. Nydén, A.-M. Hermansson, M. Rudemo, K. Braeckmans, Fluorescence recovery after photobleaching in material and life sciences: putting theory into practice, Q. Rev. Biophys. 48 (3) (2015) 323–387.
[29] M.B. Browning, T. Wilems, M.S. Hahn, E. Cosgriff-Hernandez, Compositional control of poly(ethylene glycol) hydrogel modulus independent of mesh size, J. Biomed. Mater. Res., Part A 98A (2) (2011) 268–273.

[30] D.J. Munoz-Pinto, S. Samavedi, B. Grigoryan, M.S. Hahn, Impact of secondary reactive species on the apparent decoupling of poly(ethylene glycol) diacrylate hydrogel average mesh size and modulus, Polymer 77 (2015) 227–238.
[31] E.M. Moore, J.L. West, Bioactive poly(ethylene glycol) acrylate hydrogels for regenerative engineering, Regen. Eng. Transl. Med. 5 (2) (2019) 167–179.
[32] M.P. Cuchiara, A.C.B. Allen, T.M. Chen, J.S. Miller, J.L. West, Multilayer microfluidic PEGDA hydrogels, Biomaterials 31 (21) (2010) 5491–5497.
[33] B.D. Fairbanks, M.P. Schwartz, C.N. Bowman, K.S. Anseth, Photoinitiated polymerization of PEG-diacrylate with lithium phenyl-2,4,6-trimethylbenzoylphosphinate: polymerization rate and cytocompatibility, Biomaterials 30 (35) (2009) 6702–6707.
[34] H. Liao, D. Munoz-Pinto, X. Qu, Y. Hou, M.A. Grunlan, M.S. Hahn, Influence of hydrogel mechanical properties and mesh size on vocal fold fibroblast extracellular matrix production and phenotype, Acta Biomater. 4 (5) (2008) 1161–1171.
[35] N.R. Richbourg, N.A. Peppas, Solute diffusion and partitioning in multi-arm poly (ethylene glycol) hydrogels, J. Mater. Chem. B 11 (2023) 377–388.
[36] N.R. Richbourg, A. Ravikumar, N.A. Peppas, Solute transport dependence on 3D geometry of hydrogel networks, Macromol. Chem. Phys. 222 (16) (2021), 2100138.
[37] N.R. Richbourg, N.A. Peppas, High-throughput FRAP analysis of solute diffusion in hydrogels, Macromolecules 54 (22) (2021) 10477–10486.
[38] C.-C. Lin, C.S. Ki, H. Shih, Thiol–norbornene photoclick hydrogels for tissue engineering applications, J. Appl. Polym. Sci. 132 (8) (2015).
[39] A. Raza, C.-C. Lin, The influence of matrix degradation and functionality on cell survival and morphogenesis in PEG-based hydrogels, Macromol. Biosci. 13 (8) (2013) 1048–1058.
[40] B.D. Fairbanks, M.P. Schwartz, A.E. Halevi, C.R. Nuttelman, C.N. Bowman, K. S. Anseth, A versatile synthetic extracellular matrix mimic via thiol-norbornene photopolymerization, Adv. Mater. 21 (48) (2009) 5005–5010.
[41] T. Sakai, T. Matsunaga, Y. Yamamoto, C. Ito, R. Yoshida, S. Suzuki, N. Sasaki, M. Shibayama, U.-i. Chung, Design and fabrication of a high-strength hydrogel with ideally homogeneous network structure from tetrahedron-like macromonomers, Macromolecules 41 (14) (2008) 5379–5384.
[42] L.E. Jansen, H. Kim, C.L. Hall, T.P. McCarthy, M.J. Lee, S.R. Peyton, A Poly (ethylene Glycol) Three-Dimensional Bone Marrow Hydrogel, Biomaterials, 2021, 121270.
[43] S. Galarza, A.J. Crosby, C. Pak, S.R. Peyton, Control of astrocyte quiescence and activation in a synthetic brain hydrogel, Adv. Healthcare Mater. 9 (4) (2020), 1901419.
[44] L.E. Jansen, L.J. Negrón-Piñeiro, S. Galarza, S.R. Peyton, Control of thiol-maleimide reaction kinetics in PEG hydrogel networks, Acta Biomater. 70 (2018) 120–128.
[45] N.R. Richbourg, M. Wancura, A.E. Gilchrist, S. Toubbeh, B.A.C. Harley, E. Cosgriff-Hernandez, N.A. Peppas, Precise control of synthetic hydrogel network structure via linear, independent synthesis-swelling relationships, Sci. Adv. 7 (7) (2021), eabe3245.
[46] N.R. Richbourg, N.A. Peppas, The swollen polymer network hypothesis: quantitative models of hydrogel swelling, stiffness, and solute transport, Prog. Polym. Sci. 105 (2020), 101243.
[47] N.R. Richbourg, M.K. Rausch, N.A. Peppas, Cross-evaluation of stiffness measurement methods for hydrogels, Polymer 258 (2022), 125316.
[48] Ö. Pekcan, S. Kara, Gelation mechanisms, Mod. Phys. Lett. B 26 (27) (2012), 1230019.
[49] T.-S. Lin, R. Wang, J.A. Johnson, B.D. Olsen, Revisiting the elasticity theory for real Gaussian phantom networks, Macromolecules 52 (4) (2019) 1685–1694.
[50] P. Jönsson, M.P. Jonsson, J.O. Tegenfeldt, F. Höök, A method improving the accuracy of fluorescence recovery after photobleaching analysis, Biophys. J. 95 (11) (2008) 5334–5348.
[51] V.G. Muir, S. Weintraub, A.P. Dhand, H. Fallahi, L. Han, J.A. Burdick, Influence of Microgel and Interstitial Matrix Compositions on Granular Hydrogel Composite Properties, Advanced Science n/a, 2023, 2206117 n/a.
[52] E. Schuster, K. Sott, A. Ström, A. Altskär, N. Smisdom, T. Gebäck, N. Lorén, A.-M. Hermansson, Interplay between flow and diffusion in capillary alginate hydrogels, Soft Matter 12 (17) (2016) 3897–3907.
[53] C.A. Stine, J.M. Munson, Convection-enhanced delivery: connection to and impact of interstitial fluid flow, Front. Oncol. 9 (2019).
[54] L.E. Barney, C.L. Hall, A.D. Schwartz, A.N. Parks, C. Sparages, S. Galarza, M. O. Platt, A.M. Mercurio, S.R. Peyton, Tumor cell–organized fibronectin maintenance of a dormant breast cancer population, Sci. Adv. 6 (11) (2020) eaaz4157.
[55] B. Erman, J.E. Mark, Structures and Properties of Rubberlike Networks, Oxford University Press, 1997.
[56] Y. Akagi, J.P. Gong, U.-i. Chung, T. Sakai, Transition between phantom and affine network model observed in polymer gels with controlled network structure, Macromolecules 46 (3) (2013) 1035–1040.
[57] W. Chassé, M. Lang, J.-U. Sommer, K. Saalwächter, Cross-link density estimation of PDMS networks with precise consideration of networks defects, Macromolecules 45 (2) (2012) 899–912.
[58] P.J. Flory, Theory of elasticity of polymer networks. The effect of local constraints on junctions, J. Chem. Phys. 66 (12) (1977) 5720–5729.
[59] C.W. Barney, Z. Ye, I. Sacligil, K.R. McLeod, H. Zhang, G.N. Tew, R.A. Riggleman, A.J. Crosby, Fracture of model end-linked networks, Proc. Natl. Acad. Sci. USA 119 (7) (2022), e2112389119.
[60] T. Fujiyabu, Y. Yoshikawa, U.-i. Chung, T. Sakai, Structure-property relationship of a model network containing solvent, Sci. Technol. Adv. Mater. 20 (1) (2019) 608–621.
[61] P.J. Flory, Principles of Polymer Chemistry, Cornell University Press, 1953.
[62] G.B. McKenna, F. Horkay, Effect of crosslinks on the thermodynamics of poly(vinyl alcohol) hydrogels, Polymer 35 (26) (1994) 5737–5742.
[63] J. Thakor, S. Ahadian, A. Niakan, E. Banton, F. Nasrollahi, M.M. Hasani-Sadrabadi, A. Khademhosseini, Engineered hydrogels for brain tumor culture and therapy, Bio-Des. Manuf. 3 (2020) 203–226.
[64] J. Sievers, V. Mahajan, P.B. Welzel, C. Werner, A. Taubenberger, Precision hydrogels for the study of cancer cell mechanobiology, Adv. Healthcare Mater. 12 (14) (2023), 2202514.
[65] K. Bott, Z. Upton, K. Schrobback, M. Ehrbar, J.A. Hubbell, M.P. Lutolf, S.C. Rizzi, The effect of matrix characteristics on fibroblast proliferation in 3D gels, Biomaterials 31 (32) (2010) 8454–8464.
[66] I.L. Ivanovska, J.-W. Shin, J. Swift, D.E. Discher, Stem cell mechanobiology: diverse lessons from bone marrow, Trends Cell Biol. 25 (9) (2015) 523–532.
[67] S. Bakhshandeh, H.M. Taïeb, A.R. Varadarajan, S.M. Lissek, S.M. Hücker, X. Lu, D. S. Garske, S.A.E. Young, J. Contzen, M. Gossen, S. Kirsch, J. Warfsmann, K. Honarnejad, C.A. Klein, A. Cipitria, Quiescence-inducing 3D-Engineered Matrix Uncovers Mechanosensitive and Drug Protective FHL2-P21 Signaling axis, bioRxiv, 2023, 2023.01.25.525382.
[68] B.L. LeSavage, A.E. Gilchrist, B.A. Krajina, K. Karlsson, A.R. Smith, K. Karagyozova, K.C. Klett, C. Curtis, C.J. Kuo, S.C. Heilshorn, Engineered Extracellular Matrices Reveal Stiffness-Mediated Chemoresistance in Patient-Derived Pancreatic Cancer Organoids, bioRxiv, 2022, 2022.04.22.488943.
[69] J.-W. Shin, D.J. Mooney, Extracellular matrix stiffness causes systematic variations in proliferation and chemosensitivity in myeloid leukemias, Proc. Natl. Acad. Sci. U.S.A. 113 (43) (2016) 12126–12131.
[70] E.A. Phelps, N.O. Enemchukwu, V.F. Fiore, J.C. Sy, N. Murthy, T.A. Sulchek, T. H. Barker, A.J. García, Maleimide cross-linked bioactive PEG hydrogel exhibits improved reaction kinetics and cross-linking for cell encapsulation and in situ delivery, Adv. Mater. 24 (1) (2012) 64–70.
[71] P. Dhavalikar, A. Robinson, Z. Lan, D. Jenkins, M. Chwatko, K. Salhadar, A. Jose, R. Kar, E. Shoga, A. Kannapiran, E. Cosgriff-Hernandez, Review of integrin-targeting biomaterials in tissue engineering, Adv. Healthcare Mater. 9 (23) (2020), 2000795.
[72] G. Safarians, A. Sohrabi, I. Solomon, W. Xiao, S. Bastola, B.W. Rajput, M. Epperson, I. Rosenzweig, K. Tamura, B. Singer, J. Huang, M.J. Harrison, T. Sanazzaro, M. C. Condro, H.I. Kornblum, S.K. Seidlits, Glioblastoma spheroid invasion through soft, brain-like matrices depends on hyaluronic acid–CD44 interactions, Adv. Healthcare Mater. 12 (14) (2023), 2203143.
[73] A.N. Kundu, C.E. Dougan, S. Mahmoud, A. Kilic, A. Panagiotou, N.R. Richbourg, N. Irakoze, S.R. Peyton, Tenascin-C activation of lung fibroblasts in a 3D synthetic lung extracellular matrix mimic, Adv. Mater. (2023), 2301493 n/a(n/a).
[74] B.P. Mahadik, S. Pedron Haba, L.J. Skertich, B.A.C. Harley, The use of covalently immobilized stem cell factor to selectively affect hematopoietic stem cell activity within a gelatin hydrogel, Biomaterials 67 (2015) 297–307.
[75] H. Kim, R.E. Huber, R.D. Mahapatra, N.-H. Tseng, S.R. Peyton, Tumor dormancy and relapse regulated by the extracellular matrix, in: S.P. Leong, S.D. Nathanson, J. S. Zager (Eds.), Cancer Metastasis through the Lymphovascular System, Springer International Publishing, Cham, 2022, pp. 89–96.
[76] V. Barnhouse, N. Petrikas, C. Crosby, J. Zoldan, B. Harley, Perivascular secretome influences hematopoietic stem cell maintenance in a gelatin hydrogel, Ann. Biomed. Eng. 49 (2) (2021) 780–792.
[77] M.J. Kratochvil, A.J. Seymour, T.L. Li, S.P. Paşca, C.J. Kuo, S.C. Heilshorn, Engineered materials for organoid systems, Nat. Rev. Mater. 4 (9) (2019) 606–622.
[78] A.S. Mijailovic, S. Galarza, S. Raayai-Ardakani, N.P. Birch, J.D. Schiffman, A. J. Crosby, T. Cohen, S.R. Peyton, K.J. Van Vliet, Localized characterization of brain tissue mechanical properties by needle induced cavitation rheology and volume controlled cavity expansion, J. Mech. Behav. Biomed. Mater. 114 (2020), 104168.
[79] L.E. Jansen, N.P. Birch, J.D. Schiffman, A.J. Crosby, S.R. Peyton, Mechanics of intact bone marrow, J. Mech. Behav. Biomed. Mater. 50 (2015) 299–307.
[80] E.R. Ruskowitz, C.A. DeForest, Proteome-wide analysis of cellular response to ultraviolet light for biomaterial synthesis and modification, ACS Biomater. Sci. Eng. 5 (5) (2019) 2111–2116.
[81] E.R. Ruskowitz, C.A. DeForest, Photoresponsive biomaterials for targeted drug delivery and 4D cell culture, Nat. Rev. Mater. 3 (2) (2018), 17087.
[82] P.E. Farahani, S.M. Adelmund, J.A. Shadish, C.A. DeForest, Photomediated oxime ligation as a bioorthogonal tool for spatiotemporally-controlled hydrogel formation and modification, J. Mater. Chem. B 5 (23) (2017) 4435–4442.
[83] R. Rizzo, N. Petelinšek, A. Bonato, M. Zenobi-Wong, From free-radical to radical-free: a paradigm shift in light-mediated biofabrication, Adv. Sci. 10 (8) (2023), 2205302.
[84] M.S. Rehmann, J.I. Luna, E. Maverakis, A.M. Kloxin, Tuning microenvironment modulus and biochemical composition promotes human mesenchymal stem cell tenogenic differentiation, J. Biomed. Mater. Res. 104 (5) (2016) 1162–1174.
[85] T. Canal, N.A. Peppas, Correlation between mesh size and equilibrium degree of swelling of polymeric networks, J. Biomed. Mater. Res. 23 (10) (1989) 1183–1193.
[86] E. Axpe, D. Chan, G.S. Offeddu, Y. Chang, D. Merida, H.L. Hernandez, E.A. Appel, A multiscale model for solute diffusion in hydrogels, Macromolecules 52 (18) (2019) 6889–6897.
[87] P.J. Flory, Statistical Mechanics of Chain Molecules, Interscience, New York, 1980.